An Optimal Tracking Power Sharing Controller for Inverter-Based Generators in Grid-connected Mode

Juan F. Patarroyo-Montenegro
Electrical and Computer Eng. Dept.
University of Puerto Rico
Mayaguez, Puerto Rico
juan.patarroyo@upr.edu

Konstantinos Kampouropoulos Sustainability Unit Fundació Eurecat Manresa, Spain ORCID: 0000-0002-1466-6394 Marc Castellà Rodil
Sustainability Unit
Fundació Eurecat
Manresa, Spain
marc.castella@eurecat.org

Luis Romeral
Electronics Engineering Dept.
Universitat Politèctnica de Catalunya
Terrassa, Spain
luis.romeral@upc.edu

Fabio Andrade

Electrical and Computer Eng. Dept.

University of Puerto Rico

Mayaguez, Puerto Rico

ORCID: 0000-0002-8859-7336

Jesus D. Vasquez-Plaza
Electrical and Computer Eng. Dept.
University of Puerto Rico
Mayaguez, Puerto Rico
jesus.vasquez@upr.edu

Abstract—In this work, an optimal power sharing controller for a three-phase Inverter-based Generator (IG) in a synchronous d-q reference frame is presented. The optimization of this controller is computed using a Linear-Quadratic (LQ) tracking index that measures the tracking error. This approach has many advantages regarding to stability and robustness over classical Proportional-Integral (PI) or Proportional-Resonant (PR) controllers that use droop functions for power sharing. In addition, a comprehensive model that represents a gridconnected IG sharing power to the main grid is developed using the superposition principle. This model integrates the Voltage-Current (V-I) and power sharing dynamics in a single state space expression. To the best of our knowledge, although there have been approaches in V-I and power sharing control that improve microgrid stability and transient response, there are no formal methods that integrate both controllers as a single entity. The results of this method were compared against a known Proportional-Resonant controller that use droop functions for power sharing. Results show that the optimal power sharing controller improves transient response, improves power decoupling, and also reduces the quadratic cost associated with microgrid states and inputs.

Keywords—LQR controller, Voltage Source Inverters (VSI), microgrids (MG), optimal tracking, d-q frame.

I. INTRODUCTION

Conventional energy sources such as petroleum, coal, gas, and hydroelectric are facing challenges related to sustainability, reliability, and penetration. Renewable Energy Sources (RES) are emerging as an effective solution to address these challenges. Microgrids emerge as an organized form of integrating RES in local communities or industrial clusters. Recent advances in power electronics devices, control theory, distribution systems, and government policies make microgrids a suitable solution for generating electricity in a decentralized form. However, the intermittent nature of the RES obligates engineers to address multiple challenges regarding to microgrid implementation, penetration, and formalization.

Microgrid challenges include lack of standardization policies, power quality issues, control issues related to stability and robustness, and others [1]. From these challenges, control issues represent an important challenge to improve microgrid penetration and standardization. With the implementation of optimal control theory, microgrids' technical characteristics such as stability, performance, and efficiency may be maximized.



Fig. 1. Hierarchical Control levels in microgrids [2].

Microgrid control is typically separated into different hierarchical levels. One of the most relevant proposals of a standardized hierarchical control structure for AC and DC microgrids is presented in [2]. The author sets a baseline of all the control levels involved in a microgrid as shown in Fig. 1. V-I control level regulates inverter's output signal waveform in order to meet power quality requirements such as amplitude, frequency, and harmonic distortion. Primary control regulates power sharing between generators and the main grid. Secondary control regulates microgrid power quality that is regularly distorted by Primary control level. Finally, tertiary control manages issues related to energy markets such as microgrid power sharing to the main grid, battery managing, energy generation prediction, demand response against sudden generator changes, etc.

The microgrid control bandwidth decreases with each control level implementation. It means that V-I control has the largest bandwidth and tertiary control has the lowest bandwidth. A large bandwidth implies faster dynamics, low noise attenuation, and highly negative poles. On the other hand, a small bandwidth implies slower dynamics, high noise attenuation, and microgrid closed-loop poles near to the imaginary axis. Typically, each of these control levels is designed separately due to the apparent difference in their dynamics [3].

To regulate active and reactive power sharing of an IG to the main grid, the most common control method is to use a Proportional-Integral (PI) compensator in the d-q frame or a Proportional-Resonant (PR) compensator in the α - β frame with a droop controller for the primary control level [4], [5]. This method has become popular because it does not require the plant model to adjust the control gains. Also, this method allows to design each control level almost independently because V-I and power sharing dynamics are separated by the low-pass filter of the power calculation block shown in Fig. 2.

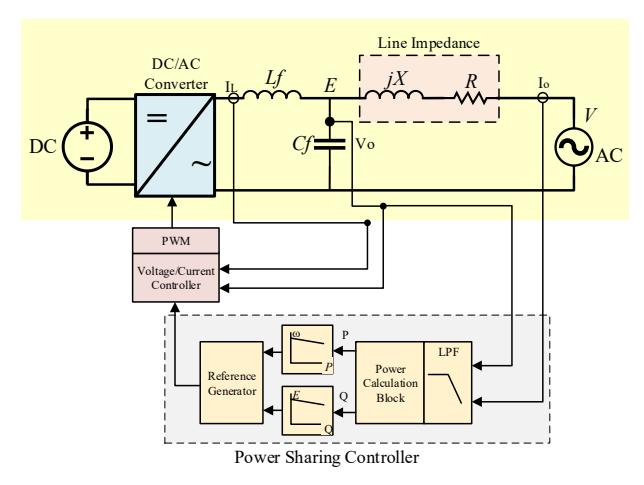


Fig. 2. Single phase inverter connected to the main grid with V-I control and power sharing droop control.

The use of droop controllers with PI or PR controllers have some drawbacks that need to be addressed such as controllability issues [6]–[8], voltage and frequency deviations [4], and line impedance sensitivity [2], [4], [9].

One of the first approaches on power sharing was developed in [10]. The author explains that active and reactive power are approximately proportional to the phase shift and voltage amplitude difference between generators. Then, a droop controller that emulated the characteristics of the synchronous generators was implemented.

In [11], a control strategy for power sharing using the classical droop method combined with the average power control method is proposed. This combination makes the system less sensitive to instantaneous voltage and current variations. In [12], a supplementary droop control loop for active power sharing is proposed. The purpose of this supplementary control loop is to address stability issues caused by the selection of high droop gains. However, the insertion of the supplementary control loop generates some nonminimum phase zeros which may affect the stability when using with higher control levels such as secondary or tertiary control. To improve transient response, a droop controller based on a small signal analysis and an extra phase shift control action was developed in [13]. The interesting contribution in this approach is the use of a small-signal model to develop a droop controller that may be used with optimal control strategies to improve transient response and guarantee robustness.

Optimal droop control methods are aimed to guarantee the best performance and/or stability margins by selecting the optimal droop gain values for active and reactive power. The main limitation that this kind of controllers have is the need of a complete open-loop mathematical model of the system. References [3], [12]–[17] provide a useful knowledge base to develop a mathematical model of an IG connected to a microgrid considering V-I and power sharing dynamics. However, these works merge inverter and controller dynamics in a single state-space model, which makes difficult to express a control law that may be optimized. In [18], The author used partial derivatives to find the optimal values of the components and constants to obtain the highest possible range of proportional droop constants. However, this approach was not aimed to improve controller performance. In [19], a virtual impedance controller [20] is used to optimize load sharing using an optimal servo LQG approach similar to [21]. However, this approach considers resonant filters that affect gain and phase margins. In [22], an optimal control approach based on Particle Swarm Optimization was developed to minimize frequency deviations in a droop controller. This method reduces active power losses but does not consider any robustness margin. In [23], an optimal controller was developed to minimize the tracking error in the output voltage of an IG. Although simulation results demonstrate to minimize tracking error and to improve harmonic distortion, this controller has limitations to be implemented in discrete-time.

This work presents an optimal power sharing controller for IG in grid-connected mode that minimizes a LO tracking index. This tracking index measures the active and reactive power deviations and also measures the energy in the control inputs. The proposed state-space model integrates V-I and power sharing dynamics by assuming a known external input that represents the main grid. The active and reactive power are calculated at the output equation of the state-space model and an optimal tracking reference is pre-computed to minimize tracking error at the output. This approach has many advantages over other approaches found in literature: First, this approach is intended to minimize the energy in the states and inputs, which means better transient response and reduced tracking error. Second, the use of a Linear Quadratic Regulator (LQR) guarantees an infinite gain margin and a minimum phase margin of 60°, which ensures robustness under disturbances in the process or sensors[24]. Third, the controller is effective on reducing active and reactive power coupling. Finally, this approach does not use resonant filters that may affect sensitivity and robustness under parameter variations.

The following section presents the mathematical model that represents the V-I and power sharing dynamics of an IG connected to the main grid using an LCL output filter. In Section III, the proposed solution for optimal power sharing tracking problem is shown. Section IV presents an example of an IG sharing power to the main grid using hardware-in-the-loop tools (HIL). Finally, the conclusion and future work are presented in Section V.

II. MATHEMATICAL MODEL

The schematic considered in this work is shown in Fig. 3. This system contains a three-phase inverter connected to the main grid using an LCL filter to attenuate switching noise. Input current, capacitor voltage and output current are symbolized by I_l , V_c , and I_o respectively.

This system has a controlled input E represented by the PWM signals that will activate each of the IGBT transistors and also has a non-controlled input V represented by the main grid. This non-controlled input is always known, and it is assumed as a three-phase signal with an amplitude of $120V_{RMS}$ and a frequency of 60Hz. The state-space model of the grid-connected inverter in the ABC frame is given by (1).

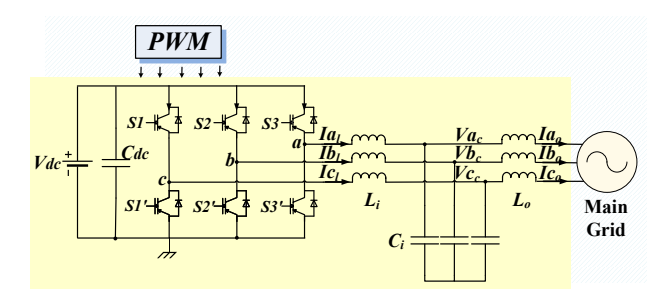


Fig. 3. Three-phase inverter connected to the main grid.

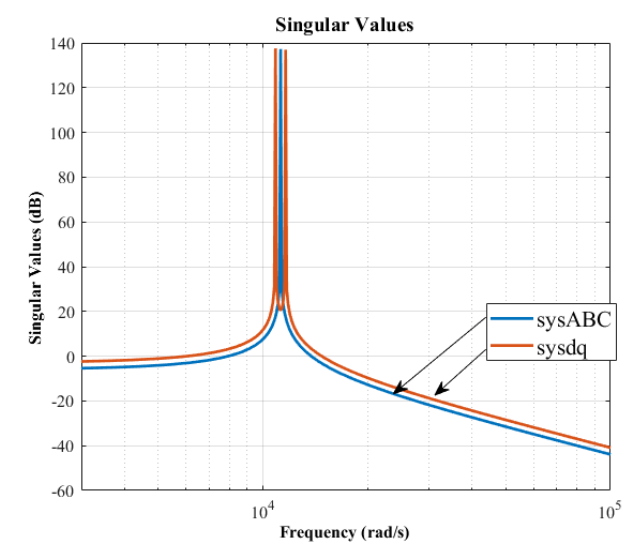


Fig. 4. Frequency response of the state-space system in ABC and d-q frame.

$$\begin{bmatrix} \dot{V}_{*c} \\ \dot{I}_{*l} \\ \dot{I}_{*o} \end{bmatrix} = \begin{bmatrix} 0 & \frac{1}{c} & -\frac{1}{c} \\ -\frac{1}{L_i} & 0 & 0 \\ \frac{1}{L_o} & 0 & 0 \end{bmatrix} \begin{bmatrix} V_{*c} \\ I_{*l} \\ I_{*o} \end{bmatrix} + \begin{bmatrix} 0 \\ L_i \\ 0 \end{bmatrix} E_* + \begin{bmatrix} 0 \\ 0 \\ -\frac{1}{Lo} \end{bmatrix} V_* \tag{1}$$

Where the subscript * represents phases A, B, or C. As main grid signal V is known, it is desired to transform the entire system to the d-q frame. This way, V may be assumed as a constant vector. To transform the entire state-space system to the d-q frame, the transformation shown in (2) should be computed for any vector z in the ABC frame.

$$z_{dq} = T_{dq} z_{ABC} \quad \text{or} \quad z_{ABC} = T_{dq}^{-1} z_{dq} \tag{2}$$

Where T_{da} is given by the well-known Clarke transformation:

$$T_{dq} = \sqrt{\frac{2}{3}} \begin{bmatrix} \cos(\omega t) & \cos\left(\omega t - \frac{2\pi}{3}\right) & \cos\left(\omega t + \frac{2\pi}{3}\right) \\ -\sin(\omega t) & -\sin\left(\omega t - \frac{2\pi}{3}\right) & -\sin\left(\omega t + \frac{2\pi}{3}\right) \\ \frac{1}{\sqrt{2}} & \frac{1}{\sqrt{2}} & \frac{1}{\sqrt{2}} \end{bmatrix}$$
(3)

Term ω is defined as the angular frequency of the rotating reference frame. Applying (2) in (1), the state-space system in the d-q frame (6) is obtained. Where the state vector is represented by $x = [V_{cd} \ V_{cq} \ I_{ld} \ I_{lq} \ I_{od} \ I_{oq}]^T$. When the reference frame is aligned with d axis, the main grid signal may be assumed as $V_{dq} = [V_d \ 0]^T$. Where V_d represents the peak amplitude of the main grid signal. A comparison of the eigenvalue frequency response between the state-space system in the ABC frame and the d-q frame using the Matlab function sigma is shown in Fig. 4. It can be noticed that there is a phase shift of $\pm \omega \ rad/s$ in the system with the d-q frame.

To integrate the power sharing dynamics, the main grid signal is assumed as a constant vector. Using the active and reactive power definition:

$$P = V_d I_d + V_q I_q$$

$$Q = V_q I_d - V_d I_q$$
(4)

The power received by the main grid may be represented in the output equation of the state-space system as follows:

$$Y = Cx = \begin{bmatrix} P \\ Q \end{bmatrix} = \begin{bmatrix} V_d & 0 \\ 0 & -V_d \end{bmatrix} \begin{bmatrix} I_{od} \\ I_{og} \end{bmatrix}$$
 (5)

It is important to remark that the system shown in (6) and (5) must be discretized in order to be implement it in a real experiment using Matlab command ss. In this case, a delay or integrator transfer function must be used to consider the delay caused by the PWM switching [25].

III. CONTROLLER DESIGN

To track the output Y[k], a discrete LQR with Optimal Reference Tracking (LQR-ORT) design method is used. The LQR-ORT control problem defines a linear-quadratic cost function that measures the system controllable input $E_{dq}[k]$ and the tracking error e[k] = Y[k] - r[k] [23][24]. The discrete LQR-ORT cost function is given by:

$$J[k_0] = \frac{1}{2} (Cx[T] - r[T])^T S[T] (Cx[T] - r[T]) + \frac{1}{2} \sum_{k=k_0}^{T} [(Y[k] - r[k])^T Q_p(Y[k] - r[k]) + E_{dq}^T [k] R_p E_{dq}[k]]$$
(7)

Where S[T] and Q_p are both symmetric and positive semidefinite matrices, and R_p is a symmetric positive definite matrix. The restriction is described by the discrete-time statespace system:

$$x[k+1] = \bar{A}_{dq}x[k] + \bar{B}_{1dq}E_{dq}[k]$$

$$Y = Cx[k]$$
(8)

Where \bar{A}_{dq} and \bar{B}_{1dq} are the discrete-time state and controllable input matrices respectively. The sub-optimal state-feedback controller matrix K_d is given by [24]:

$$K_d = \left(\bar{B}_{1dq}^T S \bar{B}_{1dq} + R_p\right)^{-1} \bar{B}_{1dq}^T S \bar{A}_{dq} \tag{9}$$

Where S is the solution to the Discrete Algebraic Ricatti Equation (DARE):

$$S = \bar{A}_{dq}^T S \left(\bar{A}_{dq} - \bar{B}_{1dq} K_d \right) + C^T Q_p C \tag{10}$$

To compute the optimal reference, the following auxiliary difference equation must be solved [24]:

$$\nu[k+1] = (\bar{A}_{dq} - \bar{B}_{1dq}K)^T \nu[k] + C_{dq}^T Q_p r[k]$$
 (11)

Solving (11) when it reaches steady-state, the following matrix ν is obtained:

$$\nu = \left[I - \left(\bar{A}_{dq} - \bar{B}_{1dq}K\right)^T\right]^{-1} C^T Q_p \tag{12}$$

$$\begin{bmatrix} V_{cd} \\ \dot{V}_{cq} \\ \dot{I}_{ld} \\ \dot{I}_{lq} \\ \dot{I}_{od} \\ \dot{I}_{lo} \\ 0 & 1/L_o & 0 & 0 & 0 & -\omega & 0 \end{bmatrix} \begin{bmatrix} V_{cd} \\ V_{cq} \\ 0 & -1/L_i & 0 & 0 & -1/c \\ 0 & -1/L_i & -\omega & 0 & 0 & 0 \\ 0 & 1/L_o & 0 & 0 & 0 & 0 & \omega \\ 0 & 1/L_o & 0 & 0 & 0 & -\omega & 0 \end{bmatrix} \begin{bmatrix} V_{cd} \\ V_{cq} \\ I_{ld} \\ I_{lq} \\ I_{od} \\ I_{oq} \end{bmatrix} + \begin{bmatrix} 0 & 0 \\ 0 & 0 \\ 0 & 1/L_i & 0 \\ 0 & 0 \\ 0 & 0 \end{bmatrix} \begin{bmatrix} E_d \\ E_q \end{bmatrix} + \begin{bmatrix} 0 & 0 \\ 0 & 0 \\ 0 & 0 \\ 0 & 0 \\ -1/L_o & 0 \\ 0 & -1/L_o \end{bmatrix} \begin{bmatrix} V_{cd} \\ V_{cq} \\ V_{cq} \\ V_{cq} \end{bmatrix}$$

$$(6)$$

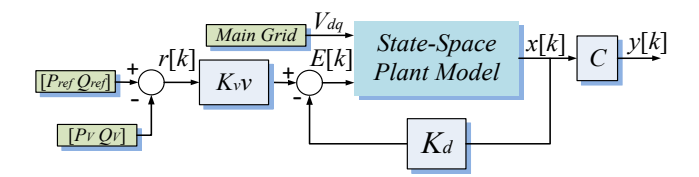


Fig. 6. Control scheme for the LQR-ORT controller with known external input.

The steady state matrix ν results in the sub-optimal reference that will be added to the controller output as follows:

$$E_{dq} = -K_d x[k] + K_v v r[k] \tag{13}$$

Where $K_v = (\bar{B}_{1dq}^T S \bar{B}_{1dq} + R_p)^{-1} \bar{B}_{1dq}^T$ is associated with the closed-loop system dynamics. According to the superposition principle, the power shared to the grid is equal to the sum of the power generated by the controllable input E_{dq} and the noncontrollable input V_{dq} .

To analyze the power generated by V_{dq} , the closed-loop system with the LQR-ORT must be simulated offline with $E_{dq} = [0\ 0]^T$ by solving the following difference equation with infinite horizon:

$$x[k+1] = (\bar{A}_{dq} - \bar{B}_{1dq}K_d) x[k] + \bar{B}_{2dq}V_{dq}$$
 (14)

Then, the power contribution of V_{dq} is computed using the following expression:

$$Y_{V} = \begin{bmatrix} P_{V} \\ Q_{V} \end{bmatrix} = \begin{bmatrix} V_{d} & 0 \\ 0 & -V_{d} \end{bmatrix} \begin{bmatrix} \bar{I}_{od} \\ \bar{I}_{og} \end{bmatrix}$$
(15)

Where \bar{I}_{od} and \bar{I}_{oq} are the output current values when (14) reaches steady state. The reference signal r[k] is then defined as follows:

$$r[k] = \begin{bmatrix} P_{ref} \\ Q_{ref} \end{bmatrix} - \begin{bmatrix} P_V \\ Q_V \end{bmatrix} \tag{16}$$

Where P_{ref} and Q_{ref} represent the desired active and reactive power shared to the main grid. The complete control scheme is shown in Fig. 6. The process of computing the LQR-ORT controller can be described by the following algorithm:

- 1. Define a positive semi-definite matrix Q_p and a positive definite matrix R_p that meets the desired performance.
- 2. Solve the ARE in (10) to obtain the solution matrix S.
- 3. Define a desired reference signal $[P_{ref} \quad Q_{ref}]^T$.
- 4. Solve the difference equation (12) to find the matrices ν and K_{ν} .
- Evaluate the performance of the LQR-ORT controller by simulating the diagram shown in Fig. 6. Performance requirements include tracking error, switching noise attenuation, transient response, and cost function value.

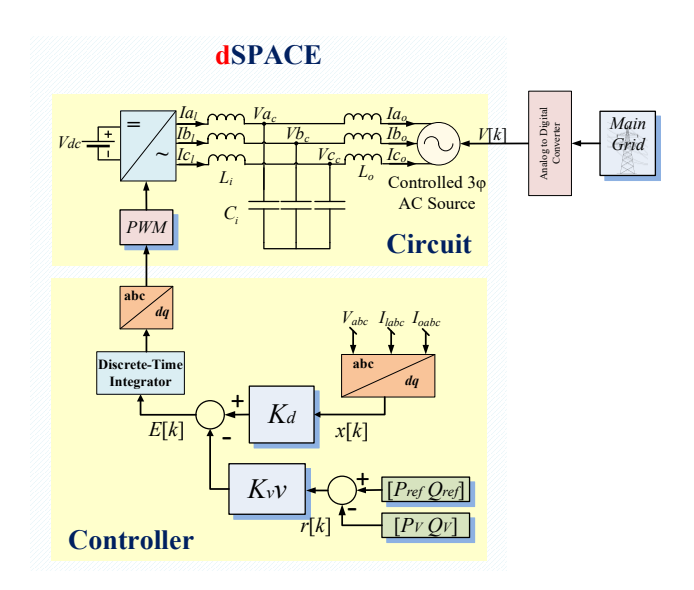


Fig. 5. Complete LQRT-ORT testing scheme using HIL.

IV. EXAMPLE

In this example, a three-phase inverter connected to the main grid with an LCL filter as described in Section II was used. The LQR-ORT controller was tested using a Hardwarein-the-loop approach with a dSPACE 1006 simulator. The complete scheme for this example is shown in Fig. 5. The main grid three-phase signal V(t) is acquired using the dSPACE digital-to-analog converter. The acquired signal V[k] is used as a reference for a simulated controlled AC source that is connected to the output of a simulated IG that is running in real time. This way, the actual grid voltage is included in the simulation in real time to evaluate controller performance under real grid conditions. In addition, this controller was compared under the same conditions against a known PR controller with droop control presented in [26]. Parameters used in this work are the same used in [26] and are presented in Table 1.

TABLE 1. CONTROL PARAMETERS FOR P-R CONTROLLER WITH DROOP CONTROL PRESENTED IN [26]

Parameter	Symbol	Value	Units							
Power Stage										
Grid Voltage	V	120	V_{RMS}							
Grid Frequency	f	60	Hz							
Output Inductance	L_o	1.8	mH							
Input Inductance	L_i	1.8	mН							
Filter Capacitance	С	8.8	μF							
Sampling Period	T_{S}	10	μs							
V-I PR Control										
Voltage Loop	k_{pV}, k_{rV}	0.35, 400								
Current Loop	k_{pi}, k_{ri}	0.7, 100								
Droop Control										
Frequency droop	k_{iP}, k_{pP}	0.0015, 0.0003								
Amplitude Droop	k_{pQ}	0.27								

	V_{cd} V_{cq} I_{ld} I_{lq} I_{od} I_{oq}	[k + 1] =	0.432 -0.016 -0.044 0.001 0.044 -0.001	0.016 0.432 -0.001 -0.044 0.001 0.044	9.085 -0.342 0.711 -0.026 0.283 -0.011	0.342 9.085 0.026 0.711 0.011 0.283	-9.113 0.343 0.283 -0.011 0.7157 -0.027	-0.343 -9.113 0.011 0.283 0.027 0.7157	0.283 -0.006 0.049 -0.008 0.005 -0.001	0.0067 0.283 0.008 0.049 0.001 0.005	$egin{array}{c} V_{cq} \ I_{ld} \ I_{lq} \ I_{od} \end{array}$	+ 0.0001	0 0 0 0 0		$\begin{bmatrix} E_d \\ E_q \end{bmatrix} +$	0.2837 -0.007 -0.005 0.001 -0.051 0.008	0.007 0.2837 -0.001 -0.005 -0.008 -0.051		(17)	
-	I_{oq}				-0.011						I_{oq}		0	- 1	LEqJ	ı		L V q J	. ,	
	E _{intd} E _{inta}			0	0 0	0	0	0	1	$\begin{bmatrix} 0 \\ 1 \end{bmatrix}$	E _{intd}		$\begin{bmatrix} 1 \\ 0 \end{bmatrix}$	$\begin{bmatrix} 0 \\ 1 \end{bmatrix}$			$\begin{bmatrix} 0 \\ 0 \end{bmatrix}$			

To include the delay of one sampling period caused by the PWM switching and to reduce tracking error, a discrete-time integrator in series with the plant model was included as follows:

$$\begin{bmatrix} x[k+1] \\ E_{int}[k+1] \end{bmatrix} = \begin{bmatrix} \bar{A}_{dq} & \bar{B}_{1dq} \\ 0 & I \end{bmatrix} \begin{bmatrix} x[k] \\ E_{int}[k] \end{bmatrix} + \begin{bmatrix} 0 \\ T_s I \end{bmatrix} E[k] \tag{18}$$

Where T_s is the sampling period. Substituting the parameters from Table 1 in (6) and discretizing using Matlab ss function, the complete state-space linear system (17) is obtained. The values of $Q=10^5I_{2\times 2}$ and $R=0.2I_{2\times 2}$ were used for the objective function (7). After solving (10) using Matlab dare function and substituting S in (9), the following value of K_d is obtained:

$$K_d = \begin{bmatrix} -0.430 & -0.027 & 5.035 & 0.334 & 3.751 & 0.254 & 1.150 & 0.017 \\ 0.027 & -0.430 & -0.334 & 5.035 & -0.254 & 3.751 & -0.017 & 1.150 \end{bmatrix}$$
(19)

The desired refence was selected to be a constant vector $[P_{ref} \quad Q_{ref}]$. Solving (11) as a difference equation yields to the optimal tracking matrix $K_{\nu}\nu$:

$$K_{\nu}\nu = \begin{bmatrix} 349.4712 & 26.6092 \\ 26.6092 & -349.4712 \end{bmatrix}^{T}$$
 (20)

To compare the results obtained in this work against a known PR-droop controller, the V-I and droop controller parameters used in [26] were used. These parameters are summarized in Table 1. Parameters k_{pi} and k_{ri} are referred to the resonant and proportional control constants for the inner current control loop. Parameters k_{pV} and k_{iV} are referred to the resonant and proportional control constants for the outer voltage control loop. Also, parameters k_{iP} , k_{pP} , and k_{pQ} are the frequency integral, frequency proportional, and amplitude proportional gains for the droop controller respectively.

Results from this example are presented in Fig. 7. To evaluate performances of both controllers, the same squared reference signals represented by RefP and RefQ were used on the LQR-ORT and the PR-droop controllers. Both signals vary from 0 to 200W and have a period of 10s. To analyze decoupling between active and reactive power, the Q_{ref} signal has a time delay of 2.5s from the P_{ref} signal.

In [26], a first-order low-pass filter at $1.25 \, rad/s$ is used to calculate the mean value of P and Q as shown in Fig. 2. This is done to reduce oscillating behavior on the droop controller and to reduce closed-loop bandwidth so that the entire converter emulates the slow dynamics of a synchronous generator. However, the small bandwidth of this filter makes difficult to analyze power transient response. The filtered values of P and Q at $1.25 \, rad/s$ for the PR-droop controller are shown in Fig. 7. To have an accurate comparison on the transient response of both controllers, a low-pass filter at $10 \, rad/s$ is used at the output of the power calculation blocks. This low-pass filter does not affect closed-loop dynamics and is only used for visualizing the mean value of P and Q. The PR-droop dynamics are not affected since the low-pass filter at $1.25 \, rad/s$ is not removed or changed.

The filtered values of P and Q at $10 \, rad/s$ for both controllers are shown in Fig. 7. It may be noticed that both controllers have a similar settling time of approximately 0.4s. However, the PR-droop controller has an overshoot with a peak value of approximately 1550W for the active power and 1550VAr for the reactive power. To address this, the PR-droop controller requires an additional low-pass filter for the reference value. This eliminates power peaks under sudden

changes in reference values but makes the closed-loop system even slower. Alternatively, the LQR-ORT controller has an over-damped response with no overshoot peaks. Also, the LQR-ORT does not require the use of a low-pass filter neither inside the control loop nor in the reference signal. Finally, it can be noticed that step changes in P generate peak values on Q and vice versa for the PR-droop controller. On the other hand, the active and reactive powers are almost decoupled with the LQR-ORT controller as evidenced in blocks B and C from Fig. 7. This decoupling is caused by the d-q synchronization, which makes the q component of the main grid signal to become zero.

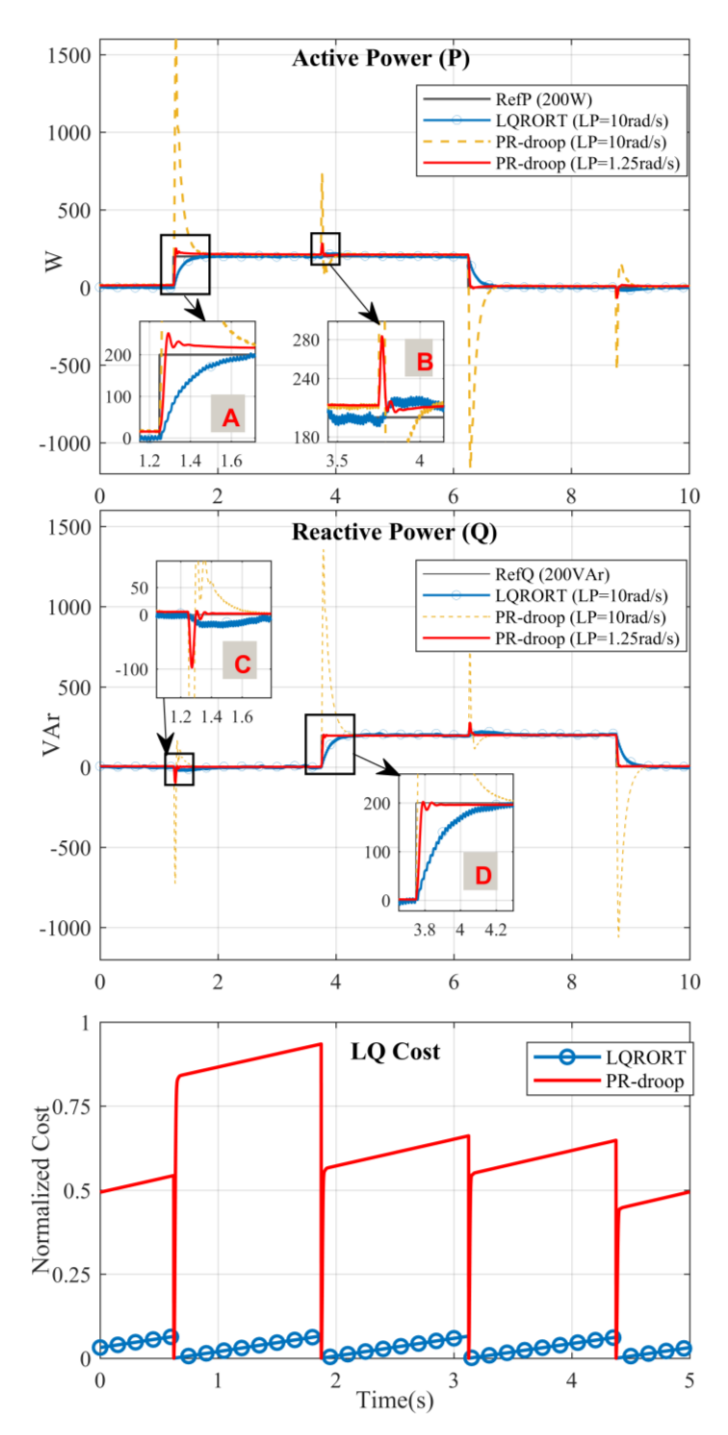


Fig. 7. Experimental results comparing the LQR-ORT controller performance with the PR-droop controller using the same reference signals. TOP: Active power. MIDDLE: Reactive Power. BOTTOM: LQ-cost values. An expanded view under reference step changes is shown in graph blocks A, B, C, and D.

The LQ cost function (7) is a dimensionless representation of the energy in the input signal and the quadratic value of the tracking error. This cost function was computed for both controllers using the same reference signals and the unfiltered P and Q values. The cost function is reset when any of the reference values RefP or RefQ have a rising or falling step. Results of this measurement are shown in the bottom section of Fig. 7. For visualization purposes, the computed values of the LO cost are normalized to a value of 2×10^5 . It can be noticed that the PR-droop controller reaches a maximum value of 0.9345 when RefP has a rising step and a maximum value of 0.66 when RefO has a rising step. On the other hand, the LQR-ORT controller reaches a maximum value of 0.065 when RefP or RefQ have a rising step. Results from the LQ cost demonstrate that the LQR-ORT controller reduces the energy in the input signal and the quadratic value of the tracking error by almost 10 times compared to the PR-droop controller.

V. CONCLUSION

This paper presents an optimal power sharing controller for a three-phase Inverter-based Generator (IG) in a synchronous d-q reference frame. The optimal controller is computed using a Linear-Quadratic cost function that measures the quadratic error and the energy in the input signal. In addition, the model for this work uses the d-q frame to transform the sinusoidal signal from the main grid into a constant vector with the q component set to zero. This allows to assume a linear system that may be used with different optimal control methods. Results demonstrate that the LQR-ORT controller does not require a low-pass filter, which improves transient response compared to a known PR-droop controller from literature. In addition, the LQR-ORT controller in the d-q frame improves decoupling between active and reactive powers. Finally, the LQR-ORT controller demonstrates to reduce the cost function, which means less quadratic error and less input energy losses. Future works include testing of the LQR-ORT in a real experiment, stability and robustness analysis, and implementation of this controller in islanded mode.

REFERENCES

- [1] H. Athari, M. Niroomand, and M. Ataei, "Review and Classification of Control Systems in Grid-tied Inverters," *Renew. Sustain. Energy Rev.*, vol. 72, no. February, pp. 1167–1176, 2017.
- [2] J. M. Guerrero, J. C. Vasquez, J. Matas, L. G. De Vicuña, and M. Castilla, "Hierarchical control of droop-controlled AC and DC microgrids A general approach toward standardization," *IEEE Trans. Ind. Electron.*, vol. 58, no. 1, pp. 158–172, 2011.
- [3] N. Pogaku, M. Prodanović, and T. C. Green, "Modeling, analysis and testing of autonomous operation of an inverter-based microgrid," *IEEE Trans. Power Electron.*, vol. 22, no. 2, pp. 613– 625, 2007.
- [4] Hr. of power sharing control strategies for islanding operation of A. microgridsua Han, X. Hou, J. Yang, J. Wu, M. Su, and J. M. Guerrero, "Review of power sharing control strategies for islanding operation of AC microgrids," *IEEE Trans. Smart Grid*, vol. 7, no. 1, pp. 200–215, 2016.
- [5] R. H. Lasseter, "MicroGrids," 2002 IEEE Power Eng. Soc. Winter Meet. Conf. Proc. (Cat. No.02CH37309), vol. 1, pp. 305–308, 2002.
- [6] C. K. Sao and P. W. Lehn, "Autonomous Load Sharing of Voltage Source Converters," *IEEE Trans. Power Deliv.*, vol. 20, no. 2, pp. 1009–1016, 2005.
- [7] C. K. Sao and P. W. Lehn, "Control and power management of converter fed microgrids," *IEEE Trans. Power Syst.*, vol. 23, no. 3, pp. 1088–1098, 2008.
- [8] U. Borup, F. Blaabjerg, and P. N. Enjeti, "Sharing of nonlinear load in parallel-connected three-phase converters," *IEEE Trans. Ind.*

- Appl., vol. 37, no. 6, pp. 1817–1823, 2001.
- [9] E. Rokrok and M. E. H. Golshan, "Adaptive voltage droop scheme for voltage source converters in an islanded multibus microgrid," *IET Gener. Transm. Distrib.*, vol. 4, no. 5, p. 562, 2010.
- [10] A. Tuladhar, H. Jin, T. Unger, and K. Mauch, "Parallel operation of single phase inverter modules with no control interconnections," in *Proceedings of APEC 97 - Applied Power Electronics Conference*, 1997, vol. 1, pp. 94–100.
- [11] M. N. Marwali, J.-W. Jung, and A. Keyhani, "Control of Distributed Generation Systems—Part II: Load Sharing Control," *IEEE Trans. Power Electron.*, vol. 19, no. 6, pp. 1551–1561, 2004.
- [12] R. Majumder, B. Chaudhuri, A. Ghosh, R. Majumder, G. Ledwich, and F. Zare, "Improvement of stability and load sharing in an autonomous microgrid using supplementary droop control loop," *IEEE Trans. Power Syst.*, vol. 25, no. 2, pp. 796–808, 2010.
- [13] H. J. Avelar, W. A. Parreira, J. B. Vieira, L. C. G. De Freitas, and E. A. A. Coelho, "A state equation model of a single-phase gridconnected inverter using a droop control scheme with extra phase shift control action," *IEEE Trans. Ind. Electron.*, vol. 59, no. 3, pp. 1527–1537, 2012.
- [14] E. A. A. Coelho, P. C. Cortizo, and P. F. D. Garcia, "Small signal stability for single phase inverter connected to stiff AC system," Conf. Rec. 1999 IEEE Ind. Appl. Conf. Thirty-Forth IAS Annu. Meet. (Cat. No.99CH36370), vol. 4, pp. 2180–2187, 1999.
- [15] E. A. A. Coelho, P. C. Cortizo, and P. F. D. Garcia, "Small-signal stability for parallel-connected inverters in stand-alone ac supply systems," *IEEE Trans. Ind. Appl.*, vol. 38, no. 2, pp. 533–542, 2002.
- [16] X. Guo, Z. Lu, B. Wang, X. Sun, L. Wang, and ..., "Dynamic Phasors-Based Modeling and Stability Analysis of Droop-Controlled Inverters for Microgrid Applications.," *IEEE Trans.* smart grid, vol. 5, no. 6, pp. 2980–2987, 2014.
- [17] R. Majumder, "Some aspects of stability in microgrids," *IEEE Trans. Power Syst.*, vol. 28, no. 3, pp. 3243–3252, 2013.
 [18] J. Zhang, J. Chen, X. Chen, and C. Gong, "Modelling, analysis and
- [18] J. Zhang, J. Chen, X. Chen, and C. Gong, "Modelling, analysis and design of droop-controlled parallel three phase voltage source inverter using dynamic phasors method," *IEEE Transp. Electrif.* Conf. Expo. ITEC Asia-Pacific 2014 - Conf. Proc., pp. 1–6, 2014.
- [19] M. Kabalan and P. Singh, "Optimizing a virtual impedance droop controller for parallel inverters," *IEEE Power Energy Soc. Gen. Meet.*, vol. 2015–Septe, 2015.
- [20] J. M. Guerrero, L. GarciadeVicuna, J. Matas, M. Castilla, and J. Miret, "Output Impedance Design of Parallel-Connected UPS Inverters With Wireless Load-Sharing Control," *IEEE Trans. Ind. Electron.*, vol. 52, no. 4, pp. 1126–1135, Aug. 2005.
- [21] C. Dirscherl, J. Fessler, C. M. Hackl, and H. Ipach, "State-feedback controller and observer design for grid-connected voltage source power converters with LCL-filter," 2015 IEEE Conf. Control Appl. CCA 2015 - Proc., pp. 215–222, 2015.
- [22] Y. A. R. I. Mohamed, H. H. Zeineldin, M. M. A. Salama, and R. Seethapathy, "Seamless formation and robust control of distributed generation microgrids via direct voltage control and optimized dynamic power sharing," *IEEE Trans. Power Electron.*, vol. 27, no. 3, pp. 1283–1294, 2012.
- [23] J. F. Patarroyo-Montenegro, J. E. Salazar-Duque, and F. Andrade, "LQR Controller with Optimal Reference Tracking for Inverter-Based Generators on Islanded-Mode Microgrids," in 2018 IEEE ANDESCON, 2018, pp. 1–5.
- [24] F. L. Lewis, D. L. Vrabie, and V. L. Syrmos, Optimal Control. Hoboken, NJ, USA: John Wiley & Sons, Inc., 2012.
- [25] M. Lu, X. Wang, P. C. Loh, F. Blaabjerg, and T. Dragicevic, "Graphical Evaluation of Time-Delay Compensation Techniques for Digitally Controlled Converters," *IEEE Trans. Power Electron.*, vol. 33, no. 3, pp. 2601–2614, 2018.
- [26] J. C. Vasquez, J. M. Guerrero, M. Savaghebi, J. Eloy-Garcia, and R. Teodorescu, "Modeling, analysis, and design of stationaryreference-frame droop-controlled parallel three-phase voltage source inverters," *IEEE Trans. Ind. Electron.*, vol. 60, no. 4, pp. 1271–1280, 2013.